



Role of N₂O and equivalence ratio on NO_x formation of methane/nitrous oxide premixed flames

Chun-Han Chen, Yueh-Heng Li*

Department of Aeronautics and Astronautics, National Cheng Kung University, Tainan 701, Taiwan, ROC



ARTICLE INFO

Article history:

Received 6 May 2020

Revised 30 September 2020

Accepted 1 October 2020

Keywords:

Nitrous oxide

NO formation

NO reaction pathway

N₂O decomposition

OPPDF

ABSTRACT

Nitrous oxide (N₂O) is often used as an oxidizer in rocket technology with plenty of potential advantages. However, the N₂O/hydrocarbon combustion results in the staggering increase of NO_x emission. To scrutinize the role of N₂O and equivalence ratio on NO formation characteristics of N₂O/CH₄ premixed flame, mixtures of N₂O/CH₄ and N₂/O₂/CH₄ were investigated by employing one-dimensional opposed-jet model with detailed reaction mechanism. The flame structures, NO reaction pathways, and NO formation routes were discussed. In the heat release rate analysis, the heat release is dominated by N₂O route, resulting in high flame temperature in N₂O/CH₄ premixed flame. Regarding the mechanism of NO formation, NO is mainly produced from N₂ through the thermal routes and from HNO through the HNO-intermediate routes for the N₂/O₂/CH₄ flame but mainly comes from N₂O through the N₂O and HNO-intermediate routes in the N₂O/CH₄ flame. The thermal routes alter to the primary chemical mechanism of NO consumption. The NO production in fuel-lean N₂O/CH₄ flames is enhanced through the N₂O route due to the increase of the mole fraction of O atom. The thermal route becomes forward reactions to produce NO for the extreme fuel-rich N₂O/CH₄ flame. Regarding the reaction pathways of the prompt route, it can be approximately divided into three categories: (1) N₂ → CN → NCN, NO (in terminal) → N₂; (2) CN → NCN, NO (in terminal) → NO, CN; (3) N₂ → CN → NCN, NO (in terminal) → N → N₂. In NO production rate analysis, the main NO formation comes from the N₂O and HNO-intermediate routes, while NO consumption associates with the thermal and NNH-intermediate routes. In addition, the prompt-NO formation is dominated by species of N₂O instead of CH radical in the extreme fuel-rich N₂O/CH₄ flames.

© 2020 The Combustion Institute. Published by Elsevier Inc. All rights reserved.

1. Introduction

With the proliferation of space industry privatization, rocket propulsion technology is anticipated to have applications to aviation for curtailing long-haul flight time and reducing fossil fuel consumption. Nitrous oxide (N₂O) is often used as an oxidizer in rocket technology because of its advantages of relatively high density-specific impulse, low toxicity, and relative high liquefaction temperature, leading to benefits in mobility and inventory [1–3]. N₂O decomposes either thermally or catalytically to 33% oxygen and 67% nitrogen (2N₂O → 2N₂ + O₂, ΔH = −163 kJ/mol). Obviously, N₂O decomposition is an exothermic reaction, and the oxygen content is higher than the normal air condition (oxygen-rich condition) [4]. Oxygen-rich conditions and high thermal exothermicity can effectively improve combustion efficiency and energy conversion [5,6]. However, N₂O is regarded as a greenhouse gas

and doubles as the main source of NO formation in the stratosphere; the presence of NO gases leads to ozone layer depletion [7]. To diminish the environmental impact, the correlation between combustion characteristics and gas emission in hydrocarbon/N₂O flames must be elucidated.

Studies on hydrocarbon combustion in the presence of nitrogen-containing oxidizers are of interest in discussing laminar burning velocity [8,9], ignition delay [10,11], and flame extinction [12,13]. There is a fair amount of literature focused on the combustion characteristics of nitrous oxides/hydrocarbon mixtures in the past. Powell et al. [14–16] examined experimentally and numerically the laminar burning velocities of N₂O flames with various hydrocarbon fuels (H₂, CH₄, C₂H₂, and C₃H₈) at near atmospheric pressure (0.8 atm). PPD mechanism, which was composed of the optimized C₁–C₃ hydrocarbon mechanism [17] and the N_xO_y/CO/H₂/O₂ chemical mechanism [18], was adopted in the numerical simulation, but the calculated laminar burning velocities from the PPD mechanism was not in agreement with the experimental data. The modified PPD mechanism, which was

* Corresponding author.

E-mail address: yueheng@mail.ncku.edu.tw (Y.-H. Li).

based on considering the most sensitive reactions with the highest rate constant uncertainty, was proposed. Pfahl et al. [19] studied the flammability limits in $H_2-CH_4-NH_3-N_2O-O_2-N_2$ mixtures. The lower and upper flammability limits for methane/nitrous oxides mixtures are 2.5–3.0% and 43–50%. In addition, the effect of small amounts of oxygen on the flammability of methane/nitrous oxides mixtures has been studied and showed that it is weak dependence on small amounts of oxygen (<5%). Wang and Zhang [20] experimentally and numerically investigated the laminar burning velocities of C_2H_4/N_2O flames, and the USM mechanism was proposed. This mechanism consists of two sub-mechanisms, which were hydrocarbon chemistry from USC Mech II-2 [21] and nitrogen chemistry from San Diego Mech [22], respectively. They modified the reaction rate constants of some critical elementary reactions, associating with N_2O and CO reaction. Nevertheless, the USM mechanism showed that it agreed well with the experimental laminar burning velocity of $CH_4/N_2O/N_2$ flame. Mével and Shepherd [23] reported the auto-ignition delay-time of hydrocarbon / N_2O mixtures by using the shock-tube technique. The ignition was driven by two reaction steps, which were $N_2O (+M) = N_2 + O (+M)$ and $N_2O + H = N_2 + OH$, for hydrocarbon/ N_2O mixtures. Newman-Lehman et al. [24] performed experimental and numerical works to elucidate the combustion behavior of $CH_4/N_2O/air$ and $C_2H_6/N_2O/air$ flames; in particular, they verified the influence of N_2O in premixed flames. The results revealed that the flame suppression effect is contingent on an increase in N_2O mass fraction in the premixed flames. Linteris et al. [25] experimentally and numerically investigated the burning velocity of CO/ N_2O premixed flames with H_2 addition. The results indicated that a direct reaction between CO and N_2O is the primary method for the consumption of these two species when the mole fraction of H_2 is less than 0.14%.

Fundamental works on the characteristics of NO_x emission for hydrocarbon fuel combustion have been investigated for several years. Sze et al. [26] studied NO_x emissions for different burner designs; Choy et al. [27] studied the pollutant emissions of opened and impinging inverse diffusion flames (IDFs) in coaxial burners. The results showed that NO_x emissions of impinging IDFs were larger than the opened IDFs one. In general, the resulting NO would be re-burnt in the post flame zone. Nonetheless, the combustion products in the post-flame zone were quenched, and the flame temperature was decreased due to the presence of the impinging wall. Therefore, the re-burned NO in the post flame zone was inhibited in impinging IDFs. Kotb and Saad [28] discussed the influence of the swirl direction on pollutant emissions and pointed out that co-swirl had higher CO_2 emissions than counter-swirl. On the other hand, counter-swirl can achieve lower NO_x emissions. In addition, Yamamoto et al. [29] explored the influence of liftoff flames on pollutant emissions. The experimental results indicated that the NO_x content decreased when the external flame was lifted. There are a certain amount of studies on the effects of dilution gas addition on pollutant emissions. Rørtveit et al. [30] investigated the influence of diluent addition on NO formation in hydrogen opposed flame. The addition of He and CO_2 can effectively reduce the NO content. On the other hand, the addition of N_2 resulted in higher NO content. Regarding the characteristics of NO_x emission for fuel/ N_2O combustion, the literature is scarce. Konnov and Dyakov [31] reported the NO emission characteristics in $CH_4/O_2/Ar$ flames doped with small amounts of N_2O . Calculated concentrations of NO significantly depends on the rate constant of reaction $N_2O + O = NO + NO$ in the fuel-lean condition.

As mentioned, few researches had examined the NO_x formation mechanism of hydrocarbon/ N_2O flames. In this study, five chemical routes associated with the NO formation mechanism [32,33] were used for numerical simulation, the thermal route, the N_2O

route, the NNH-intermediate route, the HNO-intermediate route, and the prompt route, respectively. Glarborg et al. [32] reviewed the detailed kinetic and chemical mechanism of NO formation, incorporating thermodynamic properties, reaction mechanism, and in-situ reduction of NO. Shih and Hsu [33] investigated NO_x characteristics of H_2/CO syngas counterflow diffusion flames and demonstrated the detailed reaction pathway of NO formation. As the high concentration of H_2 in syngas, most of NO was produced through the thermal route instead of the NNH-intermediate route and the N_2O route. N_2O decomposition is characterized by large exothermicity. The NO formation mechanism can thus be intuitively associated with the thermal route. However, results showed that NO converted back to N_2 through the thermal route. Nevertheless, the presence of N_2O facilitates NO formation through the HNO-intermediate route. Although the primary chemical mechanisms involved in hydrocarbon/ N_2O combustion are established, the chemical pathway of NO formation in hydrocarbon/ N_2O flames is still incomplete. Accordingly, this study conducted a detailed numerical analysis to elucidate the NO formation mechanism under the variation of CH_4/N_2O equivalence ratios. Additionally, the effect of N_2O decomposition on NO formation in a stoichiometric CH_4/N_2O flame was examined through comparison with that in a $CH_4/N_2O/O_2$ flame (with the same N–O ratio as N_2O).

2. Numerical model and chemical mechanism

This study used CHEMKIN PRO for numerical calculation, and the OPPDIF-code [34] was employed to calculate several essential properties, including the distributions of temperature, velocity, pressure, and concentration along with the axial distribution; the rates of reaction, production, and net heat release were also calculated. Furthermore, the flame configuration was analyzed using data obtained from the CHEMKIN database, such as chemical kinetics, thermodynamics, and transport properties. The physical model used in this study was a one-dimensional, counterflow premixed flame (see in [33]). The $N_2/O_2/CH_4$ and N_2O/CH_4 mixtures were respectively applied in upper and lower nozzles. The separation distance and flow rate of two nozzles were set to 2 cm and 50 cm/s, respectively. The comparisons for both mixtures were conducted at an identical strain rate of 100 s^{-1} and under ambient conditions of 300 K and 1 atm. Regarding the chemical mechanism, the chemical mechanism proposed by Glarborg et al. [32] was selected in this study. This mechanism consists of 153 species and 1397 elementary reactions, which were based on the chemistry of C_1-C_2 hydrocarbons, amines, cyanides, and interactions of hydrocarbon/nitrogen. Comprehensive mechanisms of NO formation, including the thermal NO, the prompt NO, mechanism of N_2O and NNH, oxidation of HCN, oxidation of HNCO, and oxidation of NH_3 , were also involved in this mechanism. The reaction rate constant was determined by the modified Arrhenius expression,

$$k = AT^\beta \exp\left(\frac{-E_a}{RT}\right) \quad (1)$$

where A is the pre-exponential factor, β is the temperature exponent, and E_a is the activation energy. In the simulation, to obtain converged solutions, adaptive mesh parameters were set as follows: adaptive grid control based on solution gradient (GRAD) = 0.1 and adaptive grid control based on solution curvature (CURV) = 0.1. Allowed maximum number of grid points was set as 1000, and the number of adaptive grid points was set as 20. All the simulations were considered using thermal diffusion and multicomponent transport. The discrepancy of the calculated temperature distributions in the two conditions of NTOT (allowed maximum number of grid points), that is, 1000 and 15,000, is certainly low. Therefore, the numerical results were verified to be grid-independent.

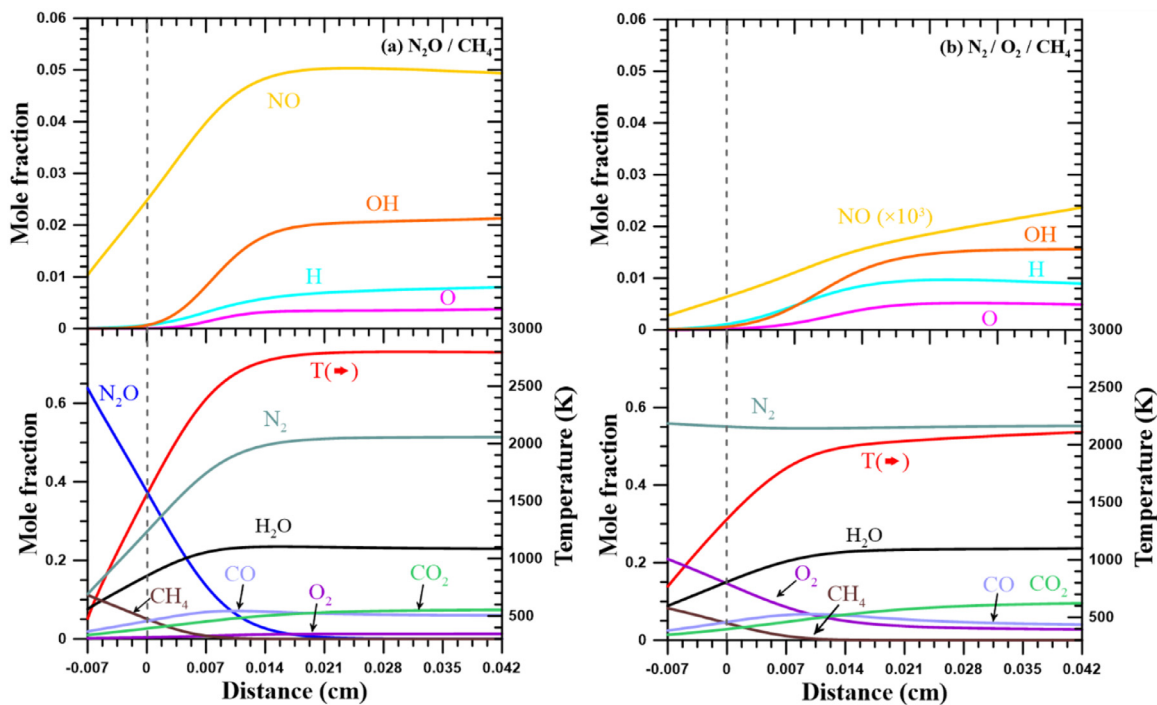


Fig. 1. Distributions of temperature and species mole fraction of (a) N_2O/CH_4 and (b) $N_2/O_2/CH_4$ flames under stoichiometric conditions.

3. Results and discussion

3.1. Effects of N_2O decomposition

N_2O decomposes to 33% O_2 and 67% N_2 at high temperatures. Therefore, to assess the role of N_2O on NO formation, two different oxidizers were prepared and compared. One of the oxidizers was pure N_2O , whilst the other comprised 33% O_2 and 67% N_2 .

Figure 1 shows the flame structures, including the distributions of temperature, and major and minor species for both N_2O/CH_4 and $N_2/O_2/CH_4$ flames under stoichiometric conditions. Because a premixed flame was applied in the opposed-jet model, the distribution was symmetrical; hence, only the left domain was displayed in Fig. 1. The dashed line represents the flame sheet denoted at locations with a maximum flame temperature gradient. The region ahead of the flame sheet defined as a preheat zone, while the region behind the flame sheet defined as a reaction zone. The results revealed that the flame temperature and mole fractions of OH were higher for the N_2O/CH_4 flame. The maximum flame temperature of the N_2O/CH_4 flame reached 2798 K, which was much higher than 2430 K for the $N_2/O_2/CH_4$ flame. For fuel consumption, CH_4 was primarily consumed through the reaction of $CH_4 + H = H_2 + CH_3$. Meanwhile, the dominant reaction of N_2O consumption was $N_2O + H = N_2 + OH$ [24]. Both N_2O and CH_4 reacted with H atom. Therefore, the mole fraction of H was low in the N_2O/CH_4 flame. In the $N_2/O_2/CH_4$ flame, the mole fraction of H was dominant in the preheat zone and the beginning portion of the reaction zone, ensuing OH mole fraction overriding after CH_4 fully completed. On the contrary, the mole fraction of OH for the N_2O/CH_4 flame was dominant in both preheat and reaction zones. It is noted that the ratio of H/OH for the N_2O/CH_4 flame was 0.40, which is certainly larger than that for the $N_2/O_2/CH_4$ flame (0.25). Moreover, the mole fractions of NO and CO were higher for the N_2O/CH_4 flame, whereas the mole fraction of CO_2 was lower. In the preheat zone, the process of N_2O consumption for its decomposition was initiated; O_2 resulting from N_2O decomposition started to react with CH_4 . After the mole fraction of CH_4 decreased to zero,

the mole fraction of CO began to decline, and the mole fraction of O_2 started to increase. It implied that fuels reacted with oxygen derived from N_2O decomposition instead of N_2O . Moreover, the mole fraction of NO increased until N_2O was consumed completely. NO formation was dominated by N_2O in the N_2O/CH_4 flame.

In order to illustrate the influence of N_2O decomposition on flame temperature, the dominant reactions of the heat release rate in both flames were shown in Fig. 2. Unlike the flame structure, as shown in Fig. 1, the distance in Fig. 2 is an absolute location, and the origin represents the nozzle exit, and the vertical dashed line represents the flame front. In the $N_2/O_2/CH_4$ premixed flame, heat release mostly comes from hydrocarbon combustion. The exothermic reaction is dominated by R78 ($O + CH_3 = H + CH_2O$), and co-dominated by R65 ($H + CH_3 (+M) = CH_4 (+M)$) and R4 ($OH + H_2 = H + H_2O$); the endothermic reaction is dominated by R1 ($H + O_2 = O + OH$). On the other hand, in the N_2O/CH_4 premixed flame, the heat release is dominated by R761 ($N_2O + H = N_2 + OH$), followed by R760 ($N_2O (+M) = N_2 + O (+M)$). Both two reactions are associated with N_2O species, and, in the meantime, these two reactions are important for NO formation in the N_2O route. The endothermic reaction was dominated by R760, whereas the exothermic reaction was dominated by the chain-propagating reaction R761. The exothermic reaction caused by R761 is much more intense than the endothermic reaction caused by R760. In order to interpret the exothermic contribution of N_2O decomposition on the resulting flame temperature, it is informative to integrate the heat release rate of specific chemical reactions along with the distance and compare the magnitudes of heat release rate for two cases. Targeted on the hydrocarbon-combustion-relevant chemical reaction, R78 is an essential reaction to contribute primary exothermicity during the combustion for two cases. Accordingly, the magnitudes of the heat release rate based on R78 are 4.03×10^{-2} kJ/cm²-s for the N_2O/CH_4 premixed flame and 6.15×10^{-2} kJ/cm²-s for the $N_2/O_2/CH_4$ premixed flame. The corresponding values are comparable. Nevertheless, in the N_2O/CH_4 premixed flame, the magnitude of the primary heat release rate based on R761 is 4.65×10^{-1} kJ/cm²-s, which is an order

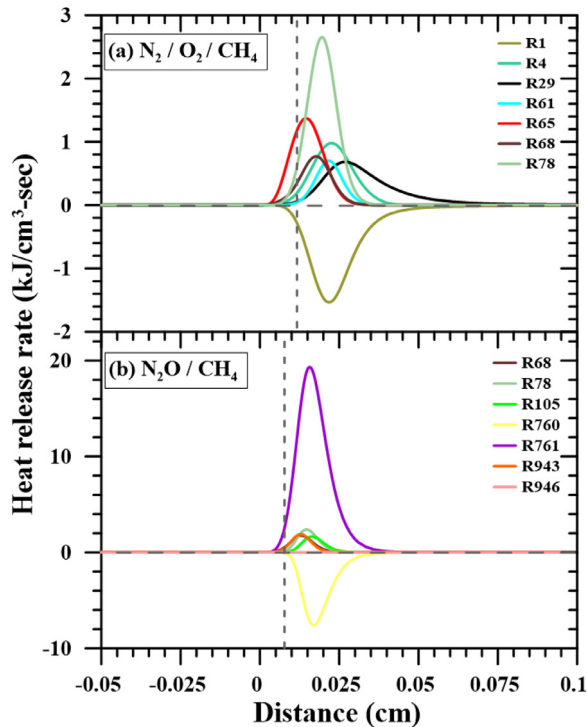


Fig. 2. The dominant reactions of heat release rate in (a) $N_2/O_2/CH_4$ and (b) N_2O/CH_4 flames under stoichiometric conditions: (R1) $H + O_2 = O + OH$; (R4) $OH + H_2 = H + H_2O$; (R29) $CO + OH = CO_2 + H$; (R61) $HCO + OH = CO + H_2O$; (R65) $CH_3 + H(+M) = CH_4(+M)$; (R68) $CH_4 + OH = CH_3 + H_2O$; (R78) $CH_3 + O = CH_2O + H$; (R105) $CH_2 + OH = CH_2O + H$; (R760) $N_2O(+M) = N_2 + O(+M)$; (R761) $N_2O + H = N_2 + OH$; (R943) $CH_2(S) + N_2O = CH_2O + N_2$; (R946) $CH + NH_3 = H_2CN + H + H$.

of magnitude greater than that of R78. Consequently, the fact of the flame temperature of the N_2O/CH_4 premixed flame much higher than that in the $N_2/O_2/CH_4$ premixed flame is attributed to the exothermicity of N_2O decomposition. It is noted that the unit of magnitudes are $kJ/cm^2 \cdot s$ instead of $kJ/cm^3 \cdot s$, because these were obtained by integrating the heat release rate along with the distance.

To study the NO formation mechanism, the net reaction rates of some major NO formation reactions for N_2O/CH_4 and $N_2/O_2/CH_4$ flames were compared under stoichiometric conditions; the results are presented in Figs. 3–6. The selected elementary reactions for NO formation are listed in Table 1. Several elementary reactions were selected from Glarborg et al. [32], namely the thermal route, the N_2O route, the NNH-intermediate route, and the prompt route, respectively. The reburning chemistry, namely the HNO-intermediate route, was also taken into consideration in the present study. The elementary reactions of the HNO-intermediate route were selected from Park and Kim [35], but those reactions can also be found from the Glarborg's mechanism. Consequently, all the reaction constants, thermodynamic, and transport data of the selected elementary reactions, including the HNO-intermediate route, were based on the mechanism proposed by Glarborg et al. [32]. The complete set of elementary reactions, including rate constants, transport data, and thermodynamic data, can be found in the Supplementary Materials. Each part of Figs. 3–6 is divided into upper and lower portions; the net reaction rates for the $N_2/O_2/CH_4$ flame are presented in the upper portions, as shown in Figs. 3(a), 4(a), 5(a) and 6(a). Those for the N_2O/CH_4 flame are presented in the lower portions, as shown in Figs. 3(b), 4(b), 5(b) and 6(b). The coordinate distances in Figs. 3–6 are absolute location. The parentheses in all of the figures represent the overall tendency of

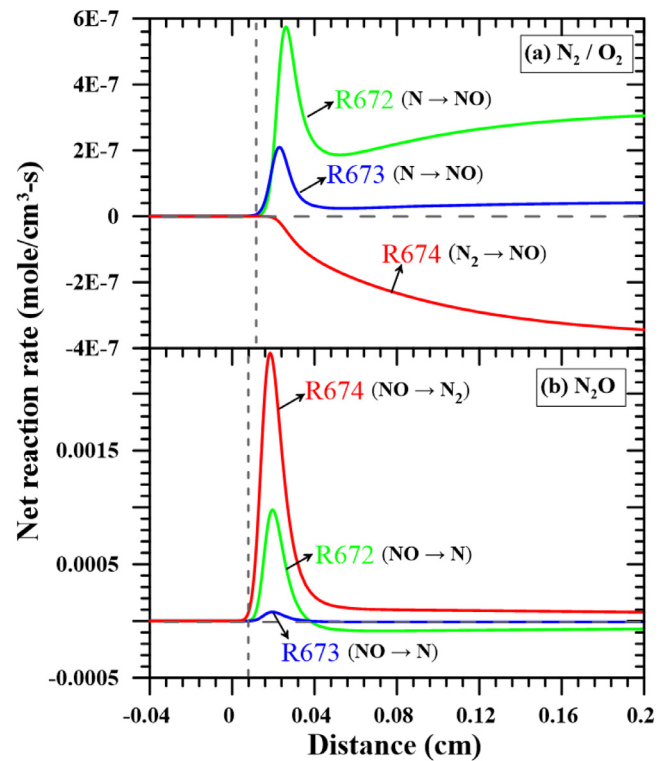


Fig. 3. Net reaction rates comparisons of NO formation reaction in the thermal route for (a) the stoichiometric $N_2/O_2/CH_4$ and (b) the stoichiometric N_2O/CH_4 flame: (R672) $N + OH = NO + H$; (R673) $N + O_2 = NO + O$; (R674) $N + NO = O + N_2$.

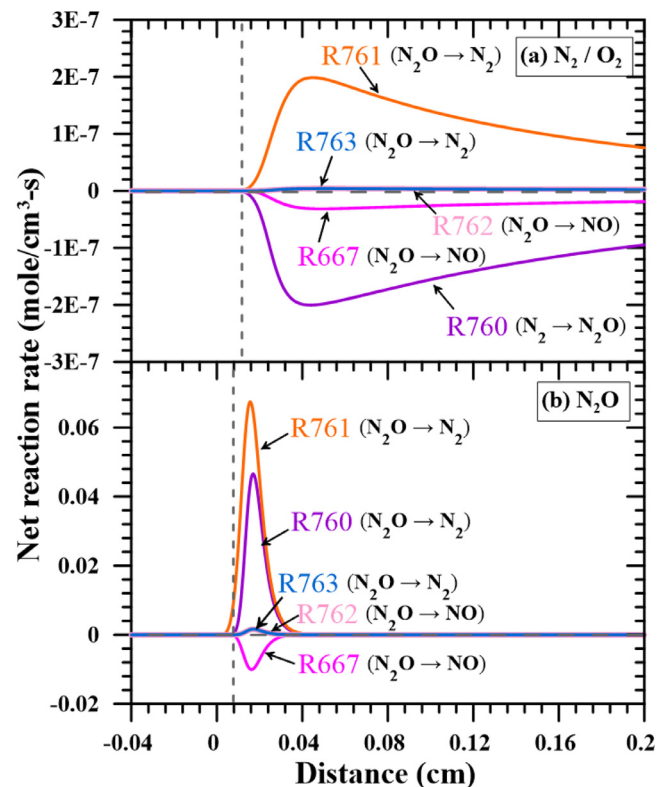


Fig. 4. Net reaction rates comparisons of NO formation reaction in the N_2O route for (a) the stoichiometric $N_2/O_2/CH_4$ and (b) the stoichiometric N_2O/CH_4 flame: (R760) $N_2O(+M) = N_2 + O(+M)$; (R761) $N_2O + H = N_2 + OH$; (R667) $NH + NO = N_2O + H$; (R762) $N_2O + O = 2NO$; (R763) $N_2O + O = N_2 + O_2$.

Table 1
Selected elementary reactions for NO formation.

Reaction number	Reaction step	A	β	E_a
<i>Thermal route</i>				
R672	$N + OH = NO + H$	3.8E13	0.000	0
R673	$N + O_2 = NO + O$	5.9E09	1.000	6280
R674	$N + NO = O + N_2$	9.4E12	0.140	0
<i>N₂O route</i>				
R760	$N_2O (+M) = N_2 + O (+M)$	9.9E10	0.000	57,901
	Low pressure limit:	6.0E14	0.000	57,444
R761	$N_2O + H = N_2 + OH$	6.4E07	1.835	13,492
R667	$NH + NO = N_2O + H$	2.7E15	-0.780	20
R762	$N_2O + O = 2NO$	9.2E13	0.000	27,679
R763	$N_2O + O = N_2 + O_2$	9.2E13	0.000	27,679
<i>NNH-intermediate route</i>				
R675	$NNH = N_2 + H$	1.0E09	0.000	0
R677	$NNH + O = N_2O + H$	1.9E14	-0.274	-22
R678	$NNH + O = N_2 + OH$	1.2E13	0.145	-217
R679	$NNH + O = NH + NO$	5.2E11	0.381	-409
R681	$NNH + O_2 = N_2 + HO_2$	5.6E14	-0.385	-13
<i>HNO-intermediate route</i>				
R720	$NO + H (+M) = HNO (+M)$	1.5E15	-0.400	0
	Low pressure limit:	2.4E14	0.206	-1550
R721	$HNO + H = NO + H_2$	6.6E10	0.9	495
R723	$HNO + OH = NO + H_2O$	1.2E09	1.200	334
<i>Prompt route</i>				
R944	$CH + N_2 = H + CN$	5.3E09	0.790	16,770
R954	$CN + N = C + N_2$	5.9E14	-0.400	0
R988	$C_2 + N_2 = 2CN$	1.5E13	0.000	41,730
R1002	$NCN + M = C + N_2 + M$	8.9E14	0.000	62,100
R1004	$NCN + H = HCN + N$	2.2E11	0.710	5321
R1005	$NCN + H = HNC + N$	4.3E-4	4.690	2434
R1006	$NCN + O = CN + NO$	2.5E13	0.170	-34
R1008	$NCN + OH = NCO + NH$	1.7E18	-1.830	4143
R1009	$NCN + OH = HCN + NO$	2.6E08	1.220	3593
R1010	$NCN + O_2 = NCO + NO$	1.3E12	0.000	23,167
R1011	$NCN + NO = CN + N_2O$	1.9E12	0.000	6280

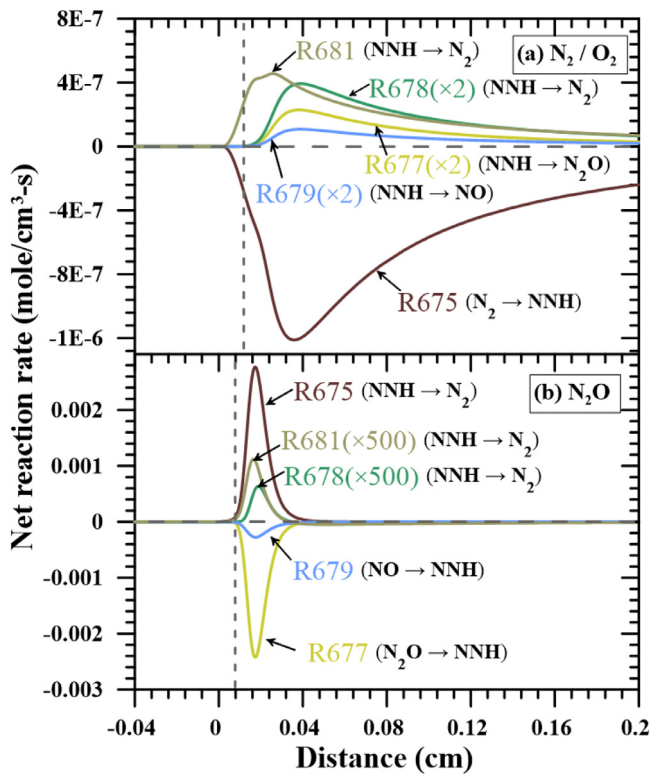


Fig. 5. Net reaction rates comparisons of NO formation reaction in the NNH-intermediate route for (a) the stoichiometric $N_2/O_2/CH_4$ and (b) the stoichiometric N_2O/CH_4 flame: (R675) $NNH=N_2+H$; (R677) $NNH+O=N_2O+H$; (R678) $NNH+O=N_2+OH$; (R679) $NNH+O=NH+NO$; (R681) $NNH+O_2=N_2+HO_2$.

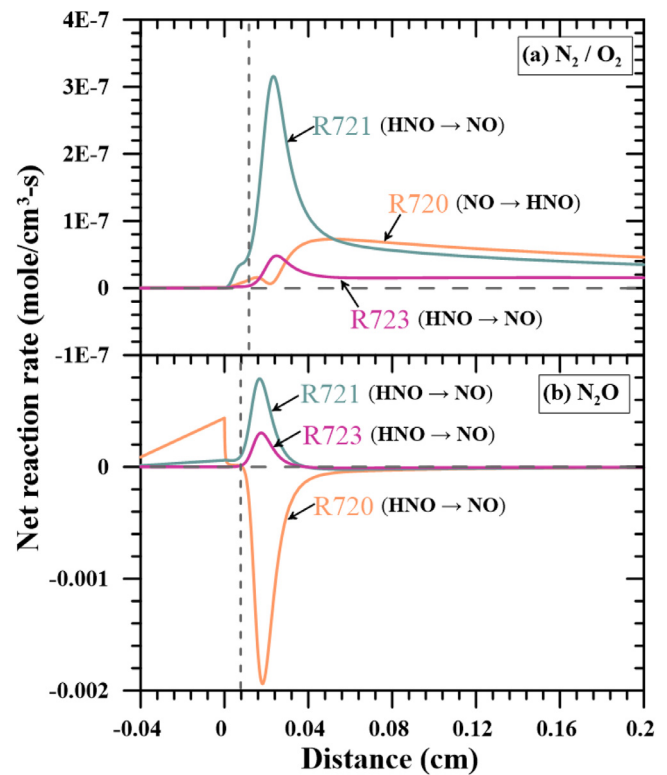


Fig. 6. Net reaction rates comparisons of NO formation reaction in the HNO-intermediate route for (a) the stoichiometric $N_2/O_2/CH_4$ and (b) the stoichiometric N_2O/CH_4 flame: (R720) $NO+H(+M)=HNO(+M)$; (R721) $HNO+H=NO+H_2$; (R723) $HNO+OH=NO+H_2O$.

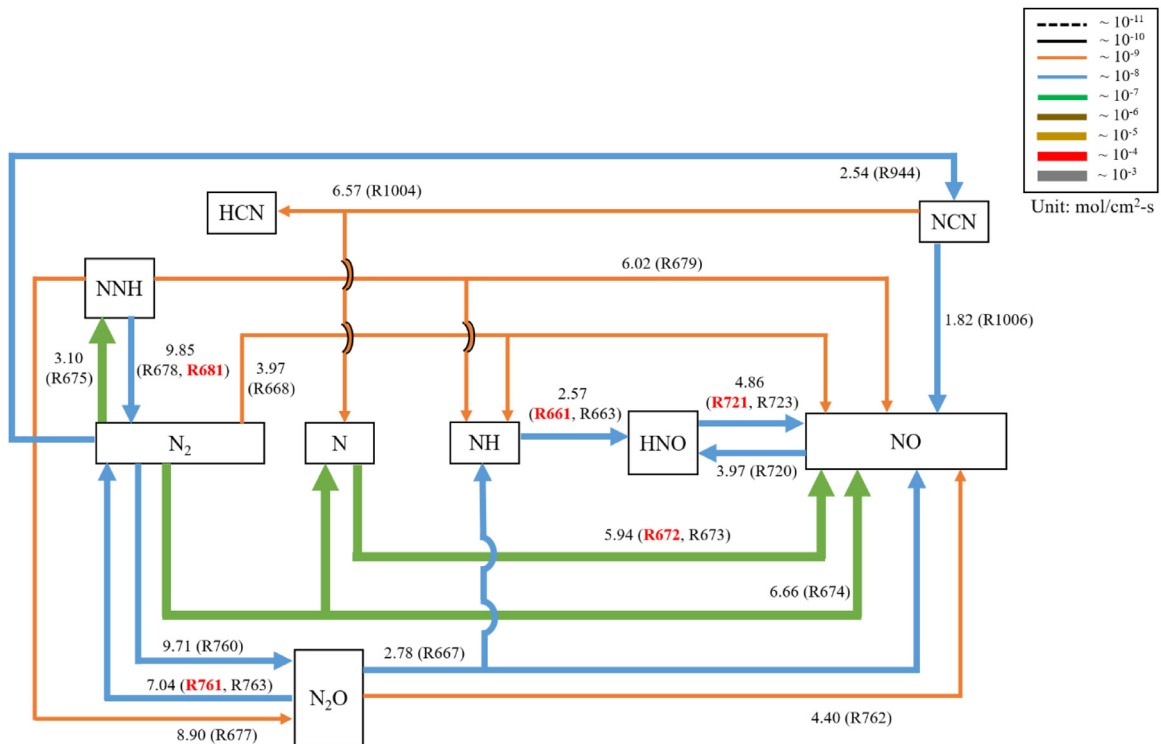


Fig. 7. The reaction pathway diagram of NO formation for the stoichiometric $N_2/O_2/CH_4$ flame. (For interpretation of the references to color in this figure, the reader is referred to the web version of this article.)

each elementary reaction, which was obtained by integrating the net reaction rate of elementary reactions along with the distance.

In Fig. 3(a) and (b), the reactions are associated with the thermal route, including R672 ($N + OH = NO + H$), R673 ($N + O_2 = NO + O$), and R674 ($N + NO = O + N_2$). For the $N_2/O_2/CH_4$ premixed flame, R672 and R674 were dominated. N_2 was converted to N and NO through reaction R674, whilst N atom became NO through R672 and R673. However, NO reacted with N to convert back to N_2 through R674 for the N_2O/CH_4 flame, as shown in Fig. 3(b). Nevertheless, at the beginning of the reaction zone, the net reaction rate of R672 and R673 had positive values, but they had shifted to negative values in the post-reaction zone ultimately, as shown in Fig. 3(b). Therefore, the overall reactions of R672 and R673 were reverse reactions, and NO was converted to N atom through these two reactions. It is noted that the net reaction rate of R673 relatively became weak for the N_2O/CH_4 flame compared to the $N_2/O_2/CH_4$ flame. It also implies that the NO formation through the thermal route for the N_2O/CH_4 flame is insignificant.

Figure 4(a) and (b) shows NO formation associated with N_2O species for both $N_2/O_2/CH_4$ and N_2O/CH_4 flames, so-called the N_2O route. For the $N_2/O_2/CH_4$ flame, N_2 became N_2O through reverse R760 ($N_2 + O (+M) \rightarrow N_2O (+M)$), and a part of N_2O may be converted back to N_2 through R761 ($N_2O + H \rightarrow N_2 + OH$) and R763 ($N_2O + O \rightarrow N_2 + O_2$). Simultaneously, N_2O was converted to NO through R762 ($N_2O + O \rightarrow 2NO$) and reverse R667 ($N_2O + H \rightarrow NH + NO$), and NO formation was dominated by reverse R667. By contrast, the overall tendency of R760 was a forward reaction ($N_2O (+M) \rightarrow N_2 + O (+M)$) instead of a reverse reaction in the N_2O/CH_4 flame; hence N_2O was converted to N_2 through R760 and R761. Since the concentration of N_2O was high at the beginning of the N_2O/CH_4 flame, this fact led R760 altering to forward reaction. NO was also formed through R762 and reverse R667 and was dominated by reverse R667. The high concentration of NO came from N_2O due to significant R667 and R762 at the beginning of N_2O/CH_4 flame, resulting in a positive net reaction rate

of R674 in the thermal route, as shown in Fig. 3(b). Also, the significant NO concentration led R672 and R673 to yield N atom in the thermal route, even if N atom became NO through R672 and R673 in the beginning of N_2O/CH_4 flame, as shown in Fig. 3(b). It is noted that R762 and R763 for both $N_2/O_2/CH_4$ and N_2O/CH_4 flames are overlapped.

Figure 5(a) and (b) illustrated NO formation through the NNH-intermediate route for both $N_2/O_2/CH_4$ and N_2O/CH_4 flames. For the $N_2/O_2/CH_4$ flame, N_2 was first converted to NNH through reverse R675 ($N_2 + H \rightarrow NNH$), which subsequently reacted with O and O_2 to convert back to N_2 through R678 ($NNH + O \rightarrow N_2 + OH$), and R681 ($NNH + O_2 \rightarrow N_2 + HO_2$), as shown in Fig. 5(a). In addition, NNH was also converted back to N_2O through R677 ($NNH + O \rightarrow N_2O + H$). For the N_2O/CH_4 flame, R675, R677, and R679 show the opposite tendency, as shown in Fig. 5(b). Since the mole fraction of N_2 in the beginning of $N_2/O_2/CH_4$ flame is larger than that of N_2O/CH_4 flame, as shown in Fig. 1(b), it made NNH form N_2 through R675. On the other hand, a high concentration of N_2O at the beginning of the N_2O/CH_4 flame, as shown in Fig. 1(a), led N_2O to produce NNH through reverse R677. As discussed previously, the significant NO concentration at the beginning of N_2O/CH_4 flame made NO converting to NNH through reverse R679.

The NO formation mechanism through the HNO-intermediate route is illustrated in Fig. 6(a) and (b) for both $N_2/O_2/CH_4$ and N_2O/CH_4 flames. HNO was converted to NO through R721 ($HNO + H \rightarrow NO + H_2$), and R723 ($HNO + OH \rightarrow NO + H_2O$), and NO was consumed through converting back to HNO via R720 ($NO + H (+M) \rightarrow HNO (+M)$). For the N_2O/CH_4 flame, R720 became a reverse reaction, indicating that NO was consumed through the HNO-intermediate route for the N_2O/CH_4 flame.

Figures 7 and 8 illustrate the overall reaction pathway diagrams of NO formation for the $N_2/O_2/CH_4$ and the N_2O/CH_4 flames with stoichiometric conditions. The reaction values on the arrows in Figs. 7 and 8 represent overall net reaction rates, which were ob-

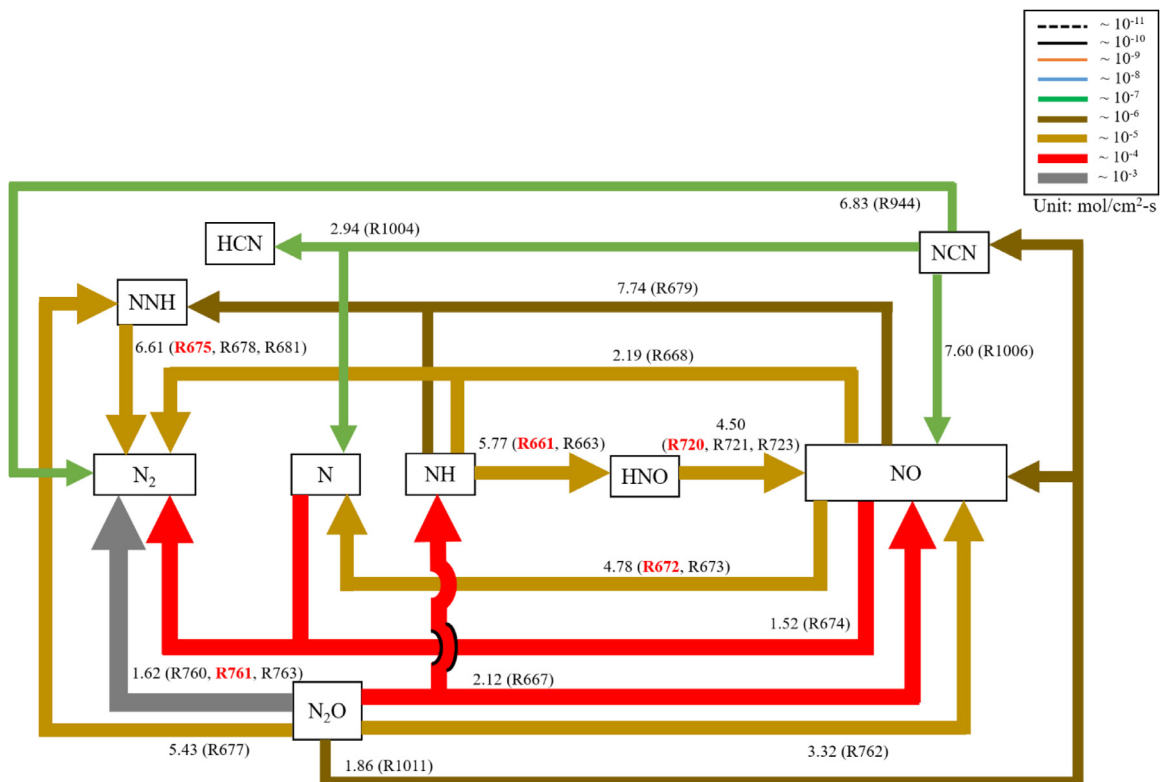


Fig. 8. The reaction pathway diagram of NO formation for the stoichiometric N_2O/CH_4 flame. (For interpretation of the references to color in this figure, the reader is referred to the web version of this article.)

tained from the integration of net reaction rate distribution over the distance between two nozzles. The reaction values marked in red denote the dominant reaction in those reactions, and the thickness of the arrows means the magnitude of the overall net reaction rate for the dominant reaction in Figs. 7 and 8. These overall reaction pathway diagrams consist of the thermal route, the N_2O route, the NNH-intermediate route, the HNO-intermediate route, and the prompt route, which were listed in Table 1. Only the dominant reactions of the prompt route presented in the overall reaction pathway diagrams, detailed reaction pathway diagrams of the prompt route are discussed in the next section. For the $N_2/O_2/CH_4$ flame, the results demonstrated that NO was mainly produced from N_2 through the thermal route (R672, R673, and reverse R674), as shown in Fig. 7. Sequentially, NO was formed from N_2 through the N_2O routes (reverse R667 and R762). In addition, the reaction pathway revealed that NH is an important species for NO formation. The formation of NH is primarily from N_2O (reverse R667), NNH (R679), and reverse R668 ($N_2 + OH \rightarrow NH + NO$), and NH is regarded as an intermediate species for NO formation through the N_2O routes. In addition, N_2 was directly consumed and formed NO through reverse R668. The species of HNO was mainly produced from NH through R661 ($NH + OH \rightarrow HNO + H$), R663 ($NH + O_2 \rightarrow HNO + O$), and was dominated by R661. HNO was then consumed through the HNO-intermediate route (R720 and R721), resulting in NO formation. N_2 was reacted with CH radical to form NCN, and sequentially NCN converted to NO through the prompt route (R944 and R1006).

Figure 8 presented the reaction pathway of NO formation in the N_2O/CH_4 flame with a stoichiometric condition. The magnitudes of overall net reaction rate for the N_2O/CH_4 flame are larger than those for the case of the $N_2/O_2/CH_4$ flame, and NO formation mainly derives from N_2O through the N_2O route (reverse R667 and R762) and the HNO-intermediate route (N_2O to NH through reverse R667, NH to HNO through R661 and HNO to NO through re-

verse R720). However, the thermal (reverse R672, reverse R673 and R674), NNH-intermediate routes (reverse R679), and R668 played the role of NO consumption in the N_2O/CH_4 flame. Moreover, N_2O was converted back to N_2 through the reaction of R761, which was the N_2O route, and the main heat release source, as shown in Fig. 2. The prompt route was presented opposite tendency in the N_2O/CH_4 flame, N_2O was consumed and formed NO and NCN through reverse R1011. Sequentially, NCN was converted to N_2 through reverse R944.

3.2. Effects of equivalence ratio

To understand the effects of equivalence ratio (ϕ) on NO formation, the N_2O/CH_4 flames were analyzed at three conditions of equivalence ratio, namely $\phi = 0.8, 1$ and 1.2 , representing fuel-lean, stoichiometric and fuel-rich conditions with a fixed flow velocity of 50 cm/s and strain rate of 100 s^{-1} . Figure 9 illustrated the distributions of minor species (H, O, and OH) at various equivalence ratios for the N_2O/CH_4 flames. The distance in Fig. 9 is absolute location, and the dash lines represent the location of the flame front. Regarding the order of minor species mole fraction, OH mole fraction was large, H mole fraction was followed, and O mole fraction was less in the stoichiometric N_2O/CH_4 flame. In the case of the fuel-lean conditions, however, OH mole fraction was still large, but O mole fraction placed second, and H mole fraction was less. On the other hand, in the case of the fuel-rich N_2O/CH_4 flame, H mole fraction was increased, but OH and O mole fraction were decreased. In the case of the stoichiometric N_2O/CH_4 flame, the numerical results indicated that the overall net reaction rate of R761 was $1.62 \times 10^{-3} \text{ mol/cm}^2\text{-s}$ (R760: $1.00 \times 10^{-3} \text{ mol/cm}^2\text{-s}$), leading to the consumption of N_2O through H atom and the yield of species N_2 and OH. While the N_2O/CH_4 mixture shifted to fuel-lean condition, the overall net reaction rate of R760 was increased to $1.15 \times 10^{-3} \text{ mol/cm}^2\text{-s}$ (R761: $1.55 \times 10^{-3} \text{ mol/cm}^2\text{-s}$), re-

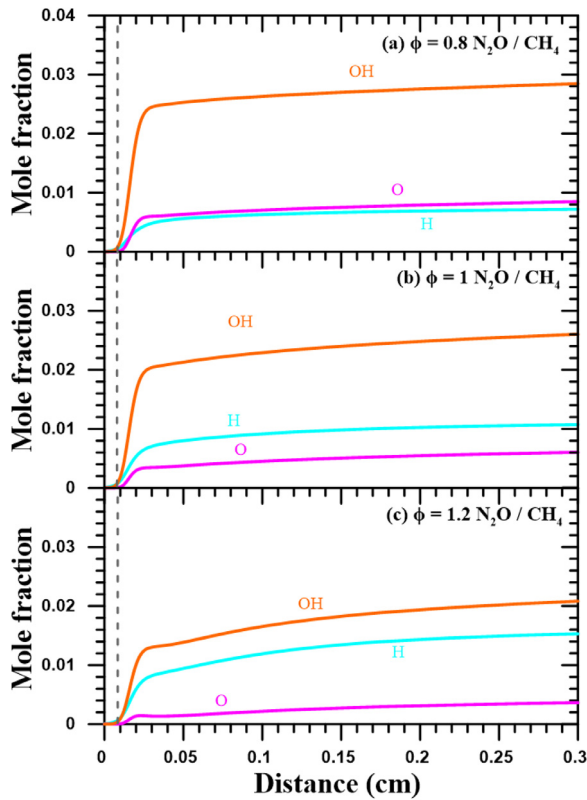


Fig. 9. The distributions of minor species (H, O, and OH) mole fraction at various equivalence ratios for the N_2O/CH_4 flame.

sulting into an increase of O atom concentration and meantime exceeding the overall amount of H mole fraction. In the meantime, a lack of N_2O in fuel-rich conditions contributed to further reduce

species N_2O and O atom, resulting in reducing OH radical but increasing H atom.

Figures 10 and 11 show the reaction pathway for the N_2O/CH_4 flame at fuel-lean ($\phi = 0.8$) and fuel-rich ($\phi = 1.2$) conditions, respectively. The reaction pathway for the fuel-lean N_2O/CH_4 flame was similar to that for the stoichiometric N_2O/CH_4 flame. The NO production through R762 and reverse R667, which are the N_2O route, was enhanced. Also, the NO formation through the HNO-intermediate route was enhanced. Comparing the mole fraction of minor species for both fuel-lean and stoichiometric conditions, as shown in Fig. 9, the mole fraction of O for fuel-lean condition increased, but the mole fractions of H decreased. Therefore, the increase of the mole fraction of O atom contributed to enhancing the reaction of R762. In addition, the consumption of NO through reverse R672 (the thermal route) was enhanced, but reverse R679 (the NNH-intermediate route) and reverse R674 (the thermal route) were reduced. For the fuel-rich N_2O/CH_4 flame, as shown in Fig. 11, N_2 was converted to NNH through reverse R678 and reverse R681, which are the NNH-intermediate route. For the NO formation through the N_2O route, the reaction of R762 became weak due to the reduction of O atom mole fraction. In addition, the magnitude of reverse R672, which led NO convert back to N_2 , was reduced. Figure 12 shows the reaction pathway diagram of NO formation for the fuel-rich N_2O/CH_4 flame at $\phi = 1.7$ with strain rate = 80 s^{-1} . For high equivalence ratio, the reactions of species N to species NO via R672 and R673, which are involved in the thermal route, became forward reactions to produce NO. It is indicated that the thermal route not only plays the role of NO consumption but also NO formation in extreme fuel-rich N_2O/CH_4 flames. Also, the formation of NO through the N_2O route (reverse R667 and R762) and HNO-intermediate route (reverse R720) was reduced, compared with the N_2O/CH_4 flame at $\phi = 1.2$. Although some of the reactions in the thermal route played the vital role of NO formation, the N_2O route was still predominant for NO formation.

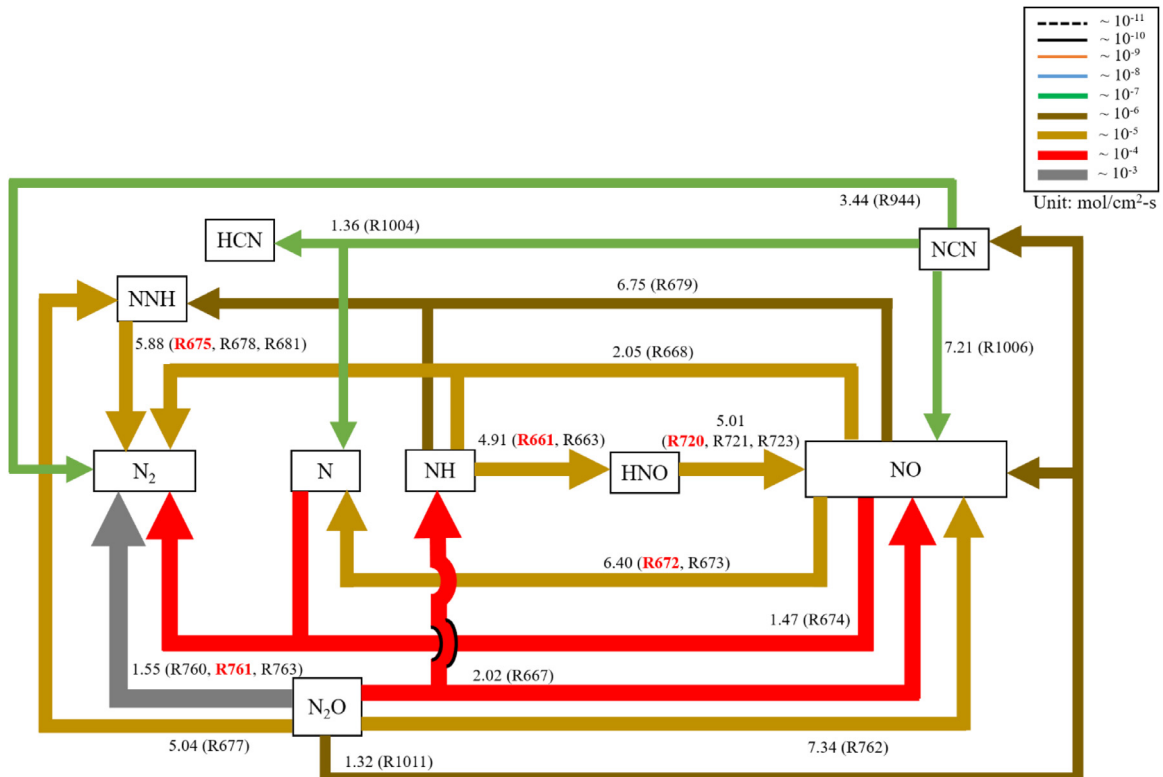


Fig. 10. The reaction pathway diagram of NO formation for the fuel-lean N_2O/CH_4 flame at $\phi = 0.8$.

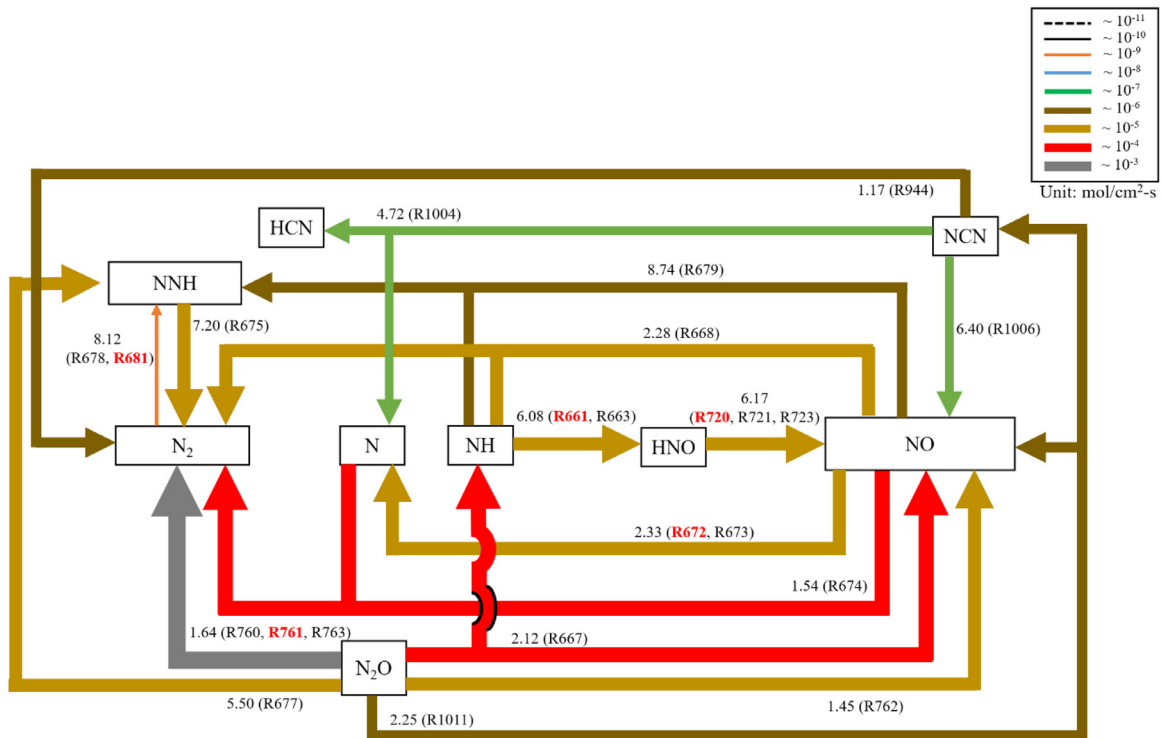


Fig. 11. The reaction pathway diagram of NO formation for the fuel-rich N_2O/CH_4 flame at $\phi = 1.2$.

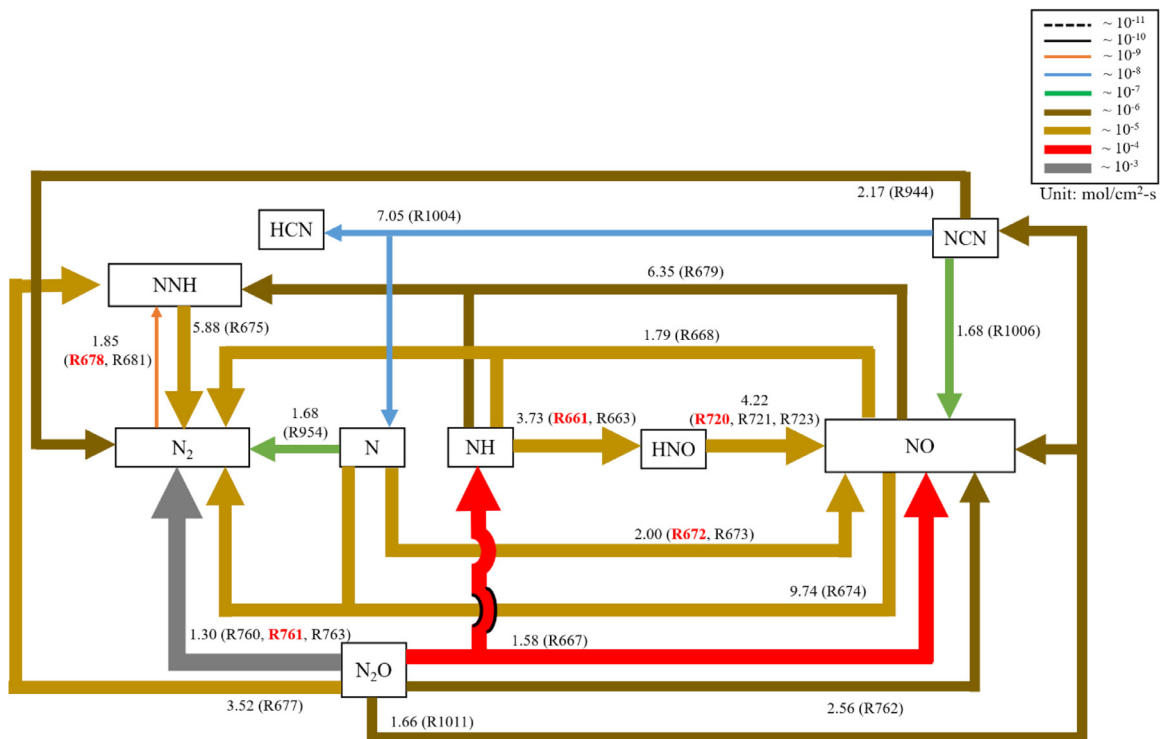


Fig. 12. The reaction pathway diagram of NO formation for the fuel-rich N_2O/CH_4 flame at $\phi = 1.7$ with strain rate = 80 s^{-1} .

Figures 13 and 14 show the reaction pathway diagram of the prompt route for stoichiometric and fuel-rich ($\phi = 1.7$) conditions with strain rate = 80 s^{-1} N_2O/CH_4 flame. For the stoichiometric N_2O/CH_4 flame, reverse R1011 ($CN + N_2O \rightarrow NCN + NO$) was the dominant reaction for NO formation. The reaction pathway diagram of the prompt route can be approximately divided into three categories: (1) $N_2 \rightarrow CN \rightarrow NCN, NO$ (in terminal) $\rightarrow N_2$; (2)

$CN \rightarrow NCN, NO$ (in terminal) $\rightarrow NO, CN$; (3) $N_2 \rightarrow CN \rightarrow NCN, NO$ (in terminal) $\rightarrow N \rightarrow N_2$. First, N_2 was reacted with C_2 to form CN through R988 ($C_2 + N_2 \rightarrow 2CN$), then N_2O was reacted with CN to form NO and NCN through reverse R1011, NCN was sequentially converted back to N_2 through reverse R944 ($H + NCN \rightarrow CH + N_2$) and R1002 ($NCN + M \rightarrow C + N_2 + M$). Second, CN was reacted to form NO and NCN through reverse R1011, then NCN

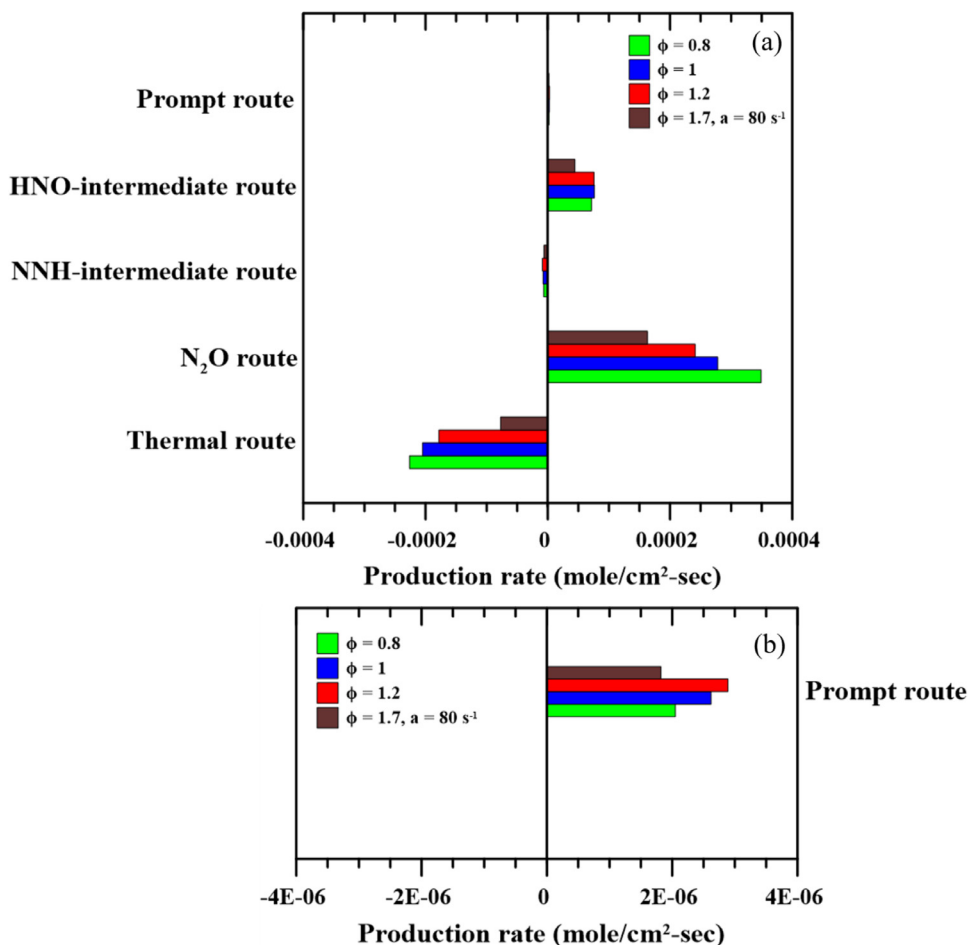


Fig. 15. Contributions of NO production rates at various equivalence ratios for $\text{N}_2\text{O}/\text{CH}_4$ flames through (a) five NO formation route and (b) only prompt route.

due to the significant concentration of H atom in high equivalence ratio conditions. In addition, the reaction of NCN to HNC and N (R1005) became a reverse reaction ($\text{HNC} + \text{N} \rightarrow \text{NCN} + \text{H}$).

Figure 15(a) shows the contributions of NO production rate based on particular NO formation routes at various equivalence ratios of the $\text{N}_2\text{O}/\text{CH}_4$ flame. The positive value represents the support of NO production, but negative value represents the support of NO consumption. In general, the main NO formation derives from the N_2O and HNO-intermediate routes, while the NO consumption came from the thermal route and NNH-intermediate routes. For NO formation, the N_2O route was predominant at the fuel-lean condition. However, while the equivalence ratio of $\text{N}_2\text{O}/\text{CH}_4$ flame changed to fuel-rich condition, the dominance of the N_2O route was reduced due to a lack of N_2O . For NO consumption, the consumption of NO through the thermal route had a similar tendency of the N_2O route, while it decreased rapidly at an extreme fuel-rich condition ($\phi = 1.7$). As discussed in Fig. 12, the reactions of species N to species NO via R672 and R673 became forward reactions to produce NO. Figure 15(b) shows NO production through prompt route at various equivalence ratios for $\text{N}_2\text{O}/\text{CH}_4$ flame. It is known that the formation of prompt-NO is significant in fuel-rich conditions due to abundant CH radicals. Indeed, the production rate of NO was increased with increasing equivalence ratio until it reached the fuel-rich condition ($\phi = 1.2$). It had a significant decrease in the extreme fuel-rich condition ($\phi = 1.7$), as shown in Fig. 15(b). In the reaction pathway diagram of the prompt route at the extreme fuel-rich condition, as shown in Fig. 14, the overall net reaction rate of the dominant reaction of NO formation (R1006,

R1010, and reverse R1011) did not increase with increasing equivalence ratio, even though reverse R944 was enhanced. It is indicated that the prompt-NO formation is dominated by species of N_2O instead of CH radical in the extreme fuel-rich $\text{N}_2\text{O}/\text{CH}_4$ flame.

4. Conclusion

The role of N_2O and equivalence ratio of $\text{N}_2\text{O}/\text{CH}_4$ mixture on NO formation characteristics were investigated by employing a one-dimensional OPPDIF program with a detailed reaction mechanism. The flame structures, NO reaction pathways, and NO formation routes were discussed. Results showed that the flame temperature and the mole fraction of OH and NO for the $\text{N}_2\text{O}/\text{CH}_4$ flame are higher than those for the $\text{N}_2/\text{O}_2/\text{CH}_4$ flame. The heat from N_2O decomposition influenced the flame temperature in $\text{N}_2\text{O}/\text{CH}_4$ premixed flames, then resulted in high flame temperature. Regarding the mechanism of NO formation, the dominant routes of NO formation are distinct in both stoichiometric $\text{N}_2/\text{O}_2/\text{CH}_4$ and $\text{N}_2\text{O}/\text{CH}_4$ flames. NO is mainly produced from N_2 through the thermal route and from HNO through the HNO-intermediate routes for the $\text{N}_2/\text{O}_2/\text{CH}_4$ flame. On the contrary, NO formation mainly comes from N_2O through the N_2O route and the HNO-intermediate route in the $\text{N}_2\text{O}/\text{CH}_4$ flame, whereas the thermal routes alter to the primary chemical mechanism of NO consumption. Even though $\text{N}_2\text{O}/\text{CH}_4$ flames demonstrated higher temperatures than $\text{N}_2/\text{O}_2/\text{CH}_4$ flames due to N_2O decomposition, the thermal route did enhance and dominate in NO consumption instead of NO formation.

The effects of equivalence ratios of N_2O/CH_4 flames on NO formation were analyzed at fuel-lean, stoichiometric, and fuel-rich conditions. The overall net reaction rate of R761 was 1.62×10^{-3} mol/cm²-s (R760: 1.00×10^{-3} mol/cm²-s), leading to the consumption of N_2O through H atom and the yield of species N_2 and OH. While the overall net reaction rate of reaction of R760 was increased to 1.15×10^{-3} mol/cm²-s in fuel-lean condition (R761: 1.55×10^{-3} mol/cm²-s in stoichiometric condition), resulting into the increase of O atom concentration and meantime exceeding the overall amount of H mole fraction. The reaction pathway for the fuel-lean N_2O/CH_4 flame is similar to that for the stoichiometric N_2O/CH_4 flame. In comparing the reaction pathway of the fuel-lean and stoichiometric N_2O/CH_4 flames, The NO production through the reaction of R762, which is the N_2O route, is enhanced due to the increase of the mole fraction of O atom. Also, the NO formation through the HNO-intermediate route was enhanced. On the other hand, the thermal route becomes forward reactions to produce NO for the N_2O/CH_4 flame at $\phi = 1.7$ with strain rate = 80 s^{-1} . It is indicated that the thermal route not only plays the role of NO consumption but also NO formation in an extreme fuel-rich N_2O/CH_4 flame. Although some of the reactions in the thermal route play the vital role of NO formation for the extreme fuel-rich condition, the N_2O route is still predominant for NO formation. Regarding the reaction pathway of the prompt route, it can be approximately divided into three categories: (1) $N_2 \rightarrow CN \rightarrow NCN$, NO (in terminal) $\rightarrow N_2$; (2) $CN \rightarrow NCN$, NO (in terminal) $\rightarrow NO$, CN; (3) $N_2 \rightarrow CN \rightarrow NCN$, NO (in terminal) $\rightarrow N \rightarrow N_2$.

Results show that the main NO formation comes from the N_2O route and the HNO-intermediate routes, while NO consumption associates with the thermal and the NNH-intermediate routes. For NO formation, the N_2O route was predominant at the fuel-lean condition. However, while the equivalence ratio of N_2O/CH_4 flame changed to fuel-rich condition, the dominance of the N_2O route was reduced due to a lack of N_2O . For NO consumption, the consumption of NO through the thermal route has a similar tendency of the N_2O route, while it decreased rapidly in the extreme fuel-rich condition ($\phi = 1.7$). The production rate of NO through the prompt route was increased with increasing equivalence ratio until it reached $\phi = 1.2$. It had a significant decrease in the extreme fuel-rich condition ($\phi = 1.7$). It is indicated that the prompt-NO formation is dominated by species of N_2O instead of CH radical in the extreme fuel-rich N_2O/CH_4 flame.

Declaration of Competing Interest

All authors declared that: (i) no support, financial or otherwise, has been received from any organization that may have an interest in the submitted work; and (ii) there are no other relationships or activities that could appear to have influenced the submitted work.

Acknowledgments

Financial support for this work was provided by the Ministry of Science and Technology (Republic of China, Taiwan) under grant numbers MOST 106-2923-E-006-003-MY3, MOST 108-2628-E-006-008-MY3, and MOST 109-2221-E-006-037-MY3. The authors wish to thank Dr. Guan-Bang Chen for numerical assistance. Computer time and numerical packages provided by the National Center for High-Performance Computing, Taiwan (NCHC Taiwan), are gratefully acknowledged.

Supplementary materials

Supplementary material associated with this article can be found, in the online version, at doi:10.1016/j.combustflame.2020.10.002.

References

- [1] G. Cai, W. Sun, J. Fang, M. Li, Y. Cong, Z. Yang, Design and performance characterization of a sub-Newton N_2O monopropellant thruster, *Aerosp. Sci. Technol.* 23 (2012) 439–451.
- [2] F. Shan, L. Hou, Y. Piao, Combustion performance and scale effect from $N_2O/HTPB$ hybrid rocket motor simulations, *Acta Astronaut.* 85 (2013) 1–11.
- [3] C. Carmicino, F. Scaramuzzino, A.R. Sorge, Trade-off between paraffin-based and aluminium-loaded HTPB fuels to improve performance of hybrid rocket fed with N_2O , *Aerosp. Sci. Technol.* 37 (2014) 81–92.
- [4] M. Galle, D. Agar, O. Watzemberger, Thermal N_2O decomposition in regenerative heat exchanger reactors, *Chem. Eng. Sci.* 56 (2001) 1587–1595.
- [5] Y.-H. Li, G.-B. Chen, Y.-C. Lin, Y.-C. Chao, Effects of flue gas recirculation on the premixed oxy-methane flames in atmospheric condition, *Energy* 89 (2015) 845–857.
- [6] G.-B. Chen, Y.-H. Li, T.-S. Cheng, Y.-C. Chao, Chemical effect of hydrogen peroxide addition on characteristics of methane–air combustion, *Energy* 55 (2013) 564–570.
- [7] J.-H. Park, J.-W. Ahn, K.-H. Kim, Y.-S. Son, Historic and futuristic review of electron beam technology for the treatment of SO_2 and NO_x in flue gas, *Chem. Eng. J.* 355 (2019) 351–366.
- [8] J. Jayachandran, A. Lefebvre, R. Zhao, F. Halter, E. Varea, B. Renou, F.N. Ego-fopoulos, A study of propagation of spherically expanding and counterflow laminar flames using direct measurements and numerical simulations, *Proc. Combust. Inst.* 35 (2015) 695–702.
- [9] E.C. Okafor, Y. Naito, S. Colson, A. Ichikawa, T. Kudo, A. Hayakawa, H. Kobayashi, Experimental and numerical study of the laminar burning velocity of CH_4-NH_3 -air premixed flames, *Combust. Flame* 187 (2018) 185–198.
- [10] E. Hu, X. Li, X. Meng, Y. Chen, Y. Cheng, Y. Xie, Z. Huang, Laminar flame speeds and ignition delay times of methane–air mixtures at elevated temperatures and pressures, *Fuel* 158 (2015) 1–10.
- [11] E. Dabora, Effect of NO_2 on the ignition delay of CH_4 -air mixtures, *Combust. Flame* 24 (1975) 181–184.
- [12] K. Maruta, M. Yoshida, Y. Ju, T. Niioka, Experimental study on methane–air premixed flame extinction at small stretch rates in microgravity, *Symp. (Int.) Combust.* 26 (1996) 1283–1289.
- [13] C. Pantano, Direct simulation of non-premixed flame extinction in a methane–air jet with reduced chemistry, *J. Fluid Mech.* 514 (2004) 231–270.
- [14] O.A. Powell, C. Dreyer, P. Papas, Laminar flame speeds of propane-nitrous oxide mixtures, 47th AIAA Aerospace Sciences Meeting Including the New Horizons Forum and Aerospace Exposition, the American Institute of Aeronautics and Astronautics (2009), p. 992.
- [15] O. Powell, J. Miller, C. Dreyer, P. Papas, Characterization of hydrocarbon/nitrous oxide propellant combinations, 46th AIAA Aerospace Sciences Meeting and Exhibit, the American Institute of Aeronautics and Astronautics (2008), p. 999.
- [16] O. Powell, P. Papas, C. Dreyer, Laminar burning velocities for hydrogen-, methane-, acetylene-, and propane-nitrous oxide flames, *Combust. Sci. Technol.* 181 (2009) 917–936.
- [17] Z. Qin, V.V. Lissianski, H. Yang, W.C. Gardiner, S.G. Davis, H. Wang, Combustion chemistry of propane: a case study of detailed reaction mechanism optimization, *Proc. Combust. Inst.* 28 (2000) 1663–1669.
- [18] M.T. Allen, R.A. Yetter, F.L. Dryer, High pressure studies of moist carbon monoxide/nitrous oxide kinetics, *Combust. Flame* 109 (1997) 449–470.
- [19] U. Pfahl, M. Ross, J. Shepherd, K. Pasamehmetoglu, C. Unal, Flammability limits, ignition energy, and flame speeds in $H_2-CH_4-NH_3-N_2O-O_2-N_2$ mixtures, *Combust. Flame* 123 (2000) 140–158.
- [20] W. Wang, H. Zhang, Laminar burning velocities of C_2H_4/N_2O flames: experimental study and its chemical kinetics mechanism, *Combust. Flame* 202 (2019) 362–375.
- [21] H. Wang, A. Laskin, A comprehensive kinetic model of ethylene and acetylene oxidation at high temperatures, Progress Report for an AFOSR New World Vista Program, (1998).
- [22] C.R. Group, The San Diego mechanism: chemical kinetic mechanisms for combustion applications Mechanical and Aerospace Engineering (Combustion Research), University of California, 2014 at <http://web.eng.ucsd.edu/mae/groups/combustion/mechanism.html>.
- [23] R. Mével, J. Shepherd, Ignition delay-time behind reflected shock waves of small hydrocarbons–nitrous oxide (–oxygen) mixtures, *Shock Waves* 25 (2015) 217–229.
- [24] T. Newman-Lehman, R. Grana, K. Seshadri, F. Williams, The structure and extinction of nonpremixed methane/nitrous oxide and ethane/nitrous oxide flames, *Proc. Combust. Inst.* 34 (2013) 2147–2153.
- [25] G.T. Linteris, M.D. Rumminger, V.I. Babushok, Premixed carbon monoxide–nitrous oxide–hydrogen flames: measured and calculated burning velocities with and without $Fe(CO)_5$, *Combust. Flame* 122 (2000) 58–75.
- [26] L. Sze, C. Cheung, C. Leung, Appearance, temperature, and NO_x emission of two inverse diffusion flames with different port design, *Combust. Flame* 144 (2006) 237–248.
- [27] Y. Choy, H. Zhen, C. Leung, H. Li, Pollutant emission and noise radiation from open and impinging inverse diffusion flames, *Appl. Energy* 91 (2012) 82–89.
- [28] A. Kotb, H. Saad, A comparison of the thermal and emission characteristics of co and counter swirl inverse diffusion flames, *Int. J. Therm. Sci.* 109 (2016) 362–373.
- [29] K. Yamamoto, S. Kato, Y. Isobe, N. Hayashi, H. Yamashita, Lifted flame structure of coannular jet flames in a triple port burner, *Proc. Combust. Inst.* 33 (2011) 1195–1201.

- [30] G.J. Rørtveit, J.E. Hustad, S.-C. Li, F.A. Williams, Effects of diluents on NO_x formation in hydrogen counterflow flames, *Combust. Flame* 130 (2002) 48–61.
- [31] A.A. Konnov, I. Dyakov, Nitrous oxide conversion in laminar premixed flames of CH₄+ O₂+ Ar, *Proc. Combust. Inst.* 32 (2009) 319–326.
- [32] P. Glarborg, J.A. Miller, B. Ruscic, S.J. Klippenstein, Modeling nitrogen chemistry in combustion, *Prog. Energy Combust. Sci.* 67 (2018) 31–68.
- [33] H.-Y. Shih, J.-R. Hsu, Computed NO_x emission characteristics of opposed-jet syngas diffusion flames, *Combust. Flame* 159 (2012) 1851–1863.
- [34] A.E. Lutz, R.J. Kee, J.F. Grcar, F.M. Rupley, OPPDIF: a Fortran program for computing opposed-flow diffusion flames, Sandia National Labs, 1997.
- [35] S. Park, Y. Kim, Effects of nitrogen dilution on the NO_x formation characteristics of CH₄/CO/H₂ syngas counterflow non-premixed flames, *Int. J. Hydrogen Energy* 42 (2017) 11945–11961.